J Mater Sci (2013) 48:7812–7826
DOI 10.1007/s10853-013-7544-x

POLYMER FIBERS

The effect of relative humidity and evaporation rate on electrospinning: fiber diameter and measurement for control implications

Yunshen Cai · Michael Gevelber

Received: 22 February 2013 / Accepted: 17 June 2013 / Published online: 17 July 2013

Abstract This paper presents an experimental study of the influence that relative humidity and evaporation rate have on the electrospinning process in terms of fiber diameter, process measurements, and selection of operating regime (applied voltage and flow rate) for polyethylene oxide/water (aqueous) solutions and poly(vinylpyrrolidone)/alcohol (non-aqueous) solutions. Poly(vinylpyrrolidone) alcohol solutions are studied to understand the separate influence of relative humidity and evaporation rate. Correlations are developed that relate measurable process parameters (jet diameter, charge density) as well as relative humidity and evaporation rate to fiber diameter. In addition, the influence that relative humidity has on selection of operating regime to achieve desired fiber diameter and maximum production rate is presented.

Introduction

Electrospinning offers a unique method to produce nanofibers from polymer solutions [1, 2], which can be used for advanced application in tissue scaffolding [3–5] and for chemical and biomedical sensors [6–9]. However, many emerging applications require the ability to achieve a desired diameter distribution and maximize production rate. Thus, it is desirable to understand what determines the fiber diameter distribution, how to determine process conditions to achieve a desired fiber diameter and what control system approach can achieve the desired fiber diameter.

Y. Cai · M. Gevelber (✉)
Department of Mechanical Engineering, Boston University, 110 Cummington St., Boston, MA 02215, USA
e-mail: gevelber@bu.edu

In a single-needle electrospinning setup, a high voltage power supply is used to create a high external electrical field and flow rate of polymer solutions into the needle is adjusted by a pump [10]. The interaction of the electrostatic forces and the surface tension of the liquid creates a "Taylor" cone [11] at the end of the needle (Fig. 1), which can be measured with a characterized volume ($\forall$) [10]. When the electrical force is larger than the surface tension, a straight jet will emerge from the Taylor cone and be accelerated due to Coulomb forces [11, 12]. The straight jet can be characterized by the jet diameter (d_{jet}) at specific length [10]. After leaving the Taylor cone, the Coulomb forces on the charges on the jet pulled against the surface tension and viscoelastic forces in the jet. With bending perturbations increasing, the straight jet will start to bend or whip at a critical point, which can be characterized in terms of a bending/whipping angle (θ) [10]. Models of electrospinning process have been developed by Yarin [13, 14], Hohman [15, 16], and Feng [17].

As De Vrieze et al. [18] suggested, the factors that affect the electrospinning processes can be divided into three groups: solution parameters, process parameters, and ambient parameters. Investigation of relationships between those three groups of parameters and the resulting fiber diameters contribute to the ability of achieving the desired fiber diameter.

Ambient RH has been identified to have a significant influence on the process by a number of researches [19–21]. Tripatanasuwan et al. [19] observed that for electrospun fibers from polyethylene oxide (PEO) aqueous solutions, increasing humidity leads to a decrease in the fiber diameters. They suggested that fiber diameter becomes smaller when evaporation and solidification rates decrease for higher ambient RH, since the jet has more stretching time. De Vrieze et al. [18] found that for electrospun fibers

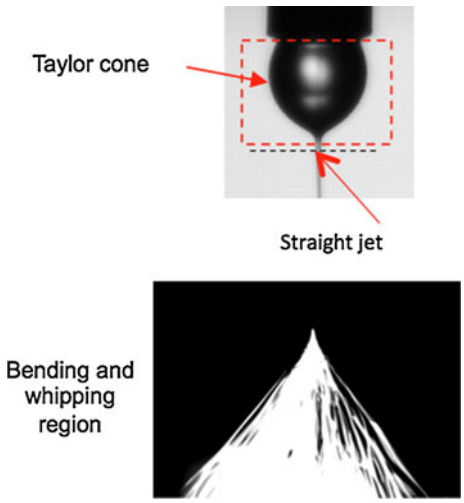

Fig. 1 Taylor cone, straight jet, and bending/whipping region of electrospinning process

from poly(vinylpyrrolidone) (PVP) non-aqueous solutions, increasing humidity also leads to a decrease in the fiber diameter, which is interesting since the alcohol solvent evaporation rate is not dependent on ambient RH. In contrast, De Vrieze et al. also observed that the electrospun nanofibers from cellulose acetate (CA) acetone/*N*,*N*-dimethylacetamide (DMAc) solutions increased as ambient RH increased. He suggested that because adding water results in a fast precipitation of the polymer for CA acetone/DMAc solutions, higher ambient RH leads to a faster precipitation rate. Similarly, Huang et al. [20] found that fiber diameters from poly(acrylonitrile) (PAN) and polysulfone (PSU) *N*,*N*-dimethylformamide solutions increased with increasing humidity. Several possible reasons were presented including: (a) that higher RH results in a decrease of the amount of excess charges on the electrospinning jet. And thus, the intensity of the electric field is decreased, resulting in a smaller stretching force. (b) More polymer precipitation occurs for higher RH level. In addition, Huang et al. found that the electrospun nanofibers from PAN and PSU solutions possess a large fiber diameter distribution.

Several researches studied the relation between process parameters, solutions parameters, and fiber diameters. Fridrikh et al. [21] derived a scaling law for polycaprolactone fibers that relates terminal fiber diameter to charge density, based on a balance between normal stresses due to surface tension and surface charge repulsion. In this analysis, viscosity is not a factor that determines final fiber diameter at the end of stretching regime since it is small related to other terms. In order to develop useful correlations between dimensionless groups that contain only measurable spinning fluid properties and measurable electrospinning parameters, Helgeson et al. [22] presented a fiber diameter correlation for PEO aqueous solutions based on a dimensionless electrostatic stress (the ratio of the electrostatic and electroviscous stresses), and a dimensionless surface stress (the ratio of the viscous stresses and surface tension). They noted that the viscous terms canceled in terms of determining fiber diameter. The fiber diameter correlation includes terms of the spinning solution conductivity, surface tension and operating parameters. However, they viewed applied flow rate is a dependent variable for the applied voltage for the process, and flow rate does not show up in those two dimensionless groups. Neither of these two correlations takes into account the influence of RH.

In terms of the upper jet diameter, Rutledge and Fridrikh [23] developed a scaling law based on balance between electrostatic and viscous terms. Although viscosity related forces are small at the end of stretching regime, viscosity plays a significant role in determining the rate of thinning of the upper jet.

In this paper, we present our experimental analysis of the relation between solution, process and ambient parameters to the resulting fiber diameter distribution and the scaling relationships between these variables. We study the impact of RH and evaporation rate on the electrospinning process and also investigate which measurable parameters can be used to correlate fiber diameters to develop an appropriate control system. Both PEO water solutions (aqueous solutions) and PVP alcohol solutions (non-aqueous solutions) are used to study the influence of RH and evaporation rate. In addition, the correlation of fiber diameter in terms of charge density, upper jet diameter are studied to determine what factors can be used as measurements for control. We also investigate the dynamics of the variations of the Taylor cone volume for different voltages, flow rates, and ambient RH to determine the operating regime bounds (relation of applied voltage and flow rate). These bounds combined with the fiber diameter correlation, can be used to determine operating regime that achieves a desired diameter and maximum production rate.

Experimental

Experiments, using PEO and PVP polymers with aqueous and non-aqueous solutions, were developed to understand the influence of RH and evaporation rate on electrospinning and the relation between measurable process parameters and fiber diameter.

Materials

PEO with 400 k average molecular weight (M_w) in water solutions and PVP with 1300 k average M_w in alcohol

solutions were used. PEO and PVP powders were purchased from the Aldrich Chemical Co. The aqueous solvents are deionized water, whose conductivity is around 0.1 μS/cm. The non-aqueous solvents are ethanol (conductivity is around 0.5 μS/cm), methanol (conductivity is around 0.9 μS/cm), and 1-butanol (conductivity is around 0.1 μS/cm), which were purchased from Sigma-Aldrich Co. The evaporation rates (Fig. 2) of those solvents were measured in an enclosed chamber at room temperature 22 °C. The evaporation rates of ethanol and methanol are ~10 times that of the evaporation rate of water, while the 1-butanol has a similar evaporation rate to water. The range of alcohol solvents evaporation rate decreases around 70 % from ethanol to 1-butanol, while the PEO powders were dissolved in deionized water to make 5, 6, and 7 wt% dilute PEO aqueous solutions. PVP powders were dissolved in different alcohol solvents to make 12 wt% PVP non-aqueous solutions. All solutions were stored in a refrigerator at 5 °C. Before experiments, solutions were put in the ambient environment for several hours to bring the solutions to room temperature (21–24 °C). In our research, all electrospinning experiments are carried out at ambient room temperature. Characteristic parameters of the solutions are given in Table 1.

Compared to the conductivities of the solvents, the conductivity of both PEO/water and PVP/alcohol solutions increases. In addition, the conductivity of 7 wt% PEO aqueous solutions is 50 times that of 12 wt% PVP/ethanol, 20 times that of 12 wt% PVP/methanol, and almost 700 times that of 12 wt% PVP/1-butanol solutions. This is consistent with the observed currents of 7 wt% PEO/water solutions (800–1400 nA) in comparison to 12 wt% PVP/ethanol solutions (35–55 nA).

The viscosity of 7 wt% PEO/water solutions is greater than that of 12 wt% PVP/alcohol solutions. This suggests that, a larger jet diameter should be observed for 7 wt% PEO/water solutions than 12 wt% PVP/alcohol solutions, which is consistent with typical 100 μm upper jet diameter for 7 wt% PEO/water solution (measured at 3 mm below vertex of needle with 28 kV applied voltage and 0.05 ml/min flow rate) to typical 60 μm for 12 wt% PVP/ethanol solution (measured at 3 mm below vertex of needle with 14 kV applied voltage and 0.05 ml/min flow rate).

This study uses two types of solutions with significantly different property values: PEO/water has 1.4 times greater surface tension, 20–700 times greater conductivity, and 8–64 times greater viscosity than different PVP/alcohol solutions. Yarin's [24] analysis indicates that Taylor cone jetting is based on the balance of surface tension, elasticity, and electrical field effects. Thus, the differences in property values are expected to have an impact on selection of operating regime (i.e., voltage range for a given flow rate that results in stable spinning), which is discussed in "Operating regime and closed-loop control system" section.

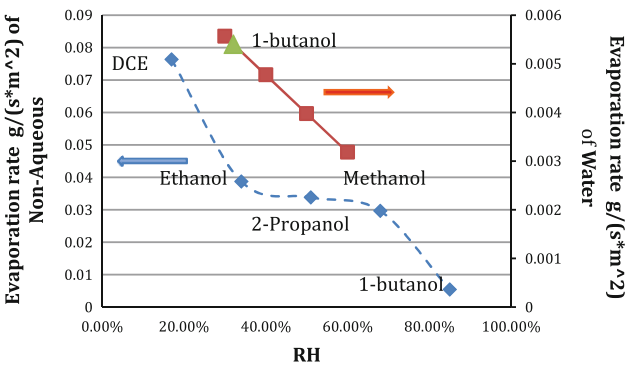

Fig. 2 Evaporation rate ranges of aqueous and non-aqueous solvents. *Dashed line* non-aqueous, *straight line* aqueous

Table 1 Typical characteristic parameters of 7 % PEO/water solutions and 12 % PVP/alcohol solutions

	Conductivity (μS/cm)	Zero shear viscosity (Pa s)	Surface tension (N/m)
7 wt% PEO/water	70	24.5	0.042
12 wt% PVP/ethanol	1.4	0.64	0.0295
12 wt% PVP/methanol	3.3	0.38	0.0305
12 wt% PVP/1-butanol	0.1	3.02	0.0301

Experimental setup

An electrospinning test-bed was developed to provide not only a basic electrospinning apparatus, but also the capability of monitoring multiple process states in real-time and setting actuator set points for the syringe pump (Harvard Apparatus, PHD 2000), high voltage power supply (HV POWER SUPPLY, XRM30P), and RH control system (Fig. 3).

In order to investigate the influence of RH, three different RH control strategies (each of which might have a different impact on electrospinning process) were developed to adjust the RH level in a chamber enclosure: (1) dry nitrogen flow; (2) water vapor; (3) salt bath. Dry nitrogen flow is applied to decrease the RH level in the enclosed chamber, when the ambient RH is higher than the required value. By adjusting the flow rate of dry nitrogen, the RH in the chamber can stay at any value that is lower than the surrounding RH level with a 10 min time constant. This approach only changes the RH in the chamber, but does not affect temperature. However, since there is a flow of gas in the chamber, it may impact the electrical charges of the system. For the water vapor system, water vapor, is generated by heated water, is infused into chamber to increase

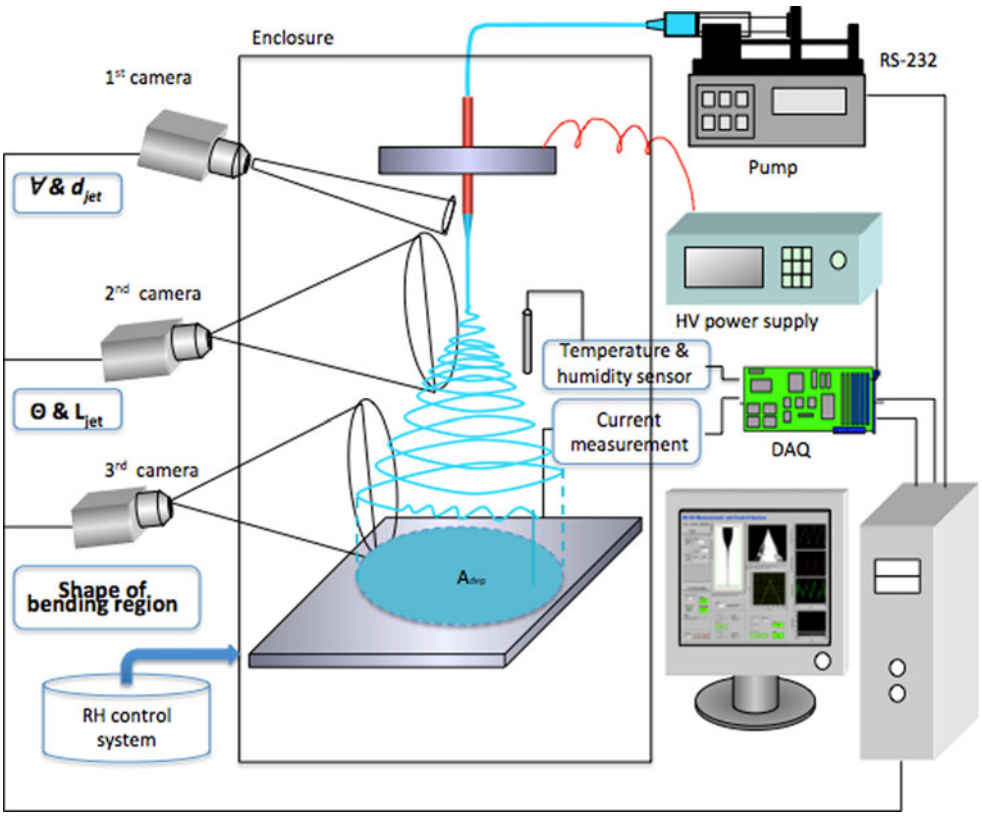

Fig. 3 Equipment schematic

the RH level when the ambient RH is lower than the required value. By adjusting the heating temperature of water, the RH in the chamber could stay at any value. But the time constant is around 30 min. This approach not only changes the RH in the chamber, but also has influence on the temperature (around 5 °C). However, the impact on airflow in the chamber is very small. To get no influence on airflow rate and temperature, a salt bath is also applied as a RH control strategy. Magnesium chloride powders (Aldrich Co.) and Magnesium nitrate Hexahydrate powders (Fluka Co.) were used to make saturated salt solutions. Each saturated salt solution possesses its own specific RH in the surrounding atmosphere. The equilibrium RH for saturated magnesium chloride salt solutions at 22 °C is 33.07 % ± 0.18 and saturated magnesium nitrate hexahydrate salt solutions at 22 °C is 54.38 % ± 0.23 [25]. Hence, only specific RH levels could be obtained by salt bath.

Figure 4 shows the measurable parameters of the system. The system can obtain image data for three major regions: (1) the Taylor cone region, (2) the upper jet region, (3) and the bending or whipping instability region. Two CCD/CMOS video camera (resolution of 3.8 μm/pix, and the field of view is around 2048 × 1552)-based vision systems were used to characterize the process states in the Taylor cone region and onset point of the bending or whipping instability region. In addition, another Canon EOS 40D camera is used to view the shape of the lower bending or whipping region. To measure fiber current (I), a current sensor is placed between the collector and the NI USB-6008 data acquisition (DAQ) card. A HTM 2500 sensor is integrated with the DAQ device to monitor both the ambient RH and temperature (T) [26, 27].

SEM analysis

The electrospun PEO and PVP fibers were imaged using a JEOL model JSM-6100 scanning electron microscope (SEM) and a Zeiss SUPRA 40VP field emission scanning electron microscope. Fibers were deposited on an aluminum foil sheet, which was placed on the fiber collector. The deposition process continues for a few minutes for each run. Then, the aluminum foil was moved into a lab hood and stored there for one day to remove the residual solvent and charge. After this drying process, the fiber samples were prepared by cutting the aluminum foil into 1 cm × 1 cm pieces and adhering them to SEM specimen stubs with carbon tape. Fiber specimens were sputter coated with an Au/Pd film for 20 s before imaging. Five to eight specimens were cut from the foil for each run to obtain the SEM images with five images taken per specimen. The number of fibers collected for diameter analysis was typically on the order of 300–600 from 40–60 SEM images. This provides a sufficient statistical significance

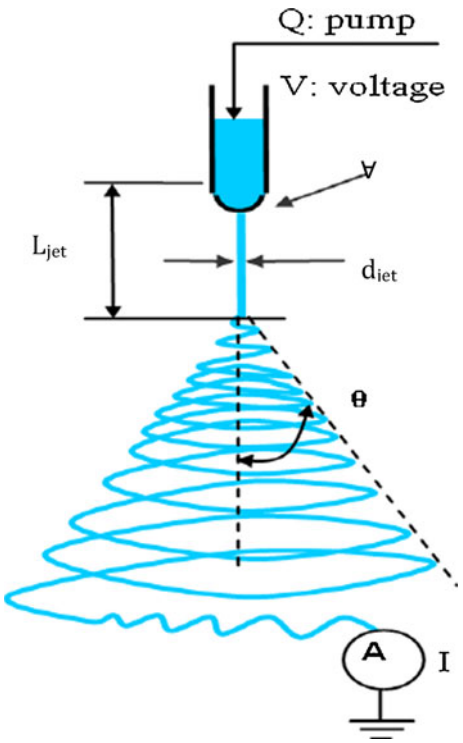

Fig. 4 Measurable process parameters

for obtaining a diameter distribution histogram. In order to assist in collecting fiber diameter data, a program utilizing LabView imaging analysis module was developed to assist in collecting, analyzing, and plotting histograms of fiber size distribution (Fig. 5) [26]. Each fiber had several measurements for obtaining true average. To track the measurement record process in the original image, the software automatically catalogs the fiber numbers, their diameter values and their standard deviation for the original image to track the measurement record process. The standard deviation of fiber diameter ($\sigma^N = \frac{\sigma}{\bar{x}}$) indicates the uniformity of fiber diameters.

Separate role of relative humidity and evaporation rate on electrospinning process

Experiments were conducted to determine the influence of RH on electrospinning for PEO/water solutions and PVP/alcohol solutions. In addition to fiber diameter, the impact of RH on measurable process variables is studied, including current, jet diameter, Taylor cone volume, and bending angle, which contribute to understanding the process physics.

PEO aqueous solutions

RH is defined as the ratio of the partial pressure of water vapor (P_∞) in an air–water mixture to the saturated vapor pressure of water (P_s) at a prescribed temperature. For constant temperature (T), the evaporation rate ($\dot{m}_{evap}$) (g/s m^2)) of the jet of aqueous solution is proportional to (1 − RH) and given by [28]:

$$\dot{m}_{evap} = (P_s - P_\infty)\beta^* \frac{M_w}{R^* T} \quad (1)$$

where β^* is the mass transfer coefficient for the evaporating liquid and geometry (m/s); M_w is the molecular weight of solutions (g/mol); R^* is the gas constant (J/(mol K)); T is the temperature in degrees Kelvin (K).

Electrospinning experiments of PEO aqueous solutions were conducted with RH ranging between 30 and 60 % at a room temperature 22 °C, corresponding to evaporation rates change from 0.0057 to 0.003 g/(s m^2) (shown in Fig. 2). Thus, as RH increases, the jet will need more time to solidify.

Figure 6 shows that both fiber diameters and current decrease as RH increases for the PEO/water solutions. Fiber diameters decrease approximately 43 %, while current decreases 30 %, as RH increases by 25 %, and evaporation rate decreases 40 %. It is interesting that the fiber diameter decreases while current also decreases, since smaller current, which indicates smaller electrical stretching force, is expected to result in a thicker upper jet. Tripatanasuwan et al. [19] suggest one possible explanation for the reduction in fiber diameter, which is that solidification of solutions happens more slowly because of the greater stretching time for higher ambient RH.

To gain insight into the process physics, the influence of RH on process parameters is studied. Figure 7 shows the effect of RH on jet diameters, Taylor cone volume, and bending angle. As RH increase from 35 to 60 %, the upper jet diameter increases 57 % and Taylor cone volumes increases 120 %, which is consistent with the 30 % decrease of current. However, RH has little influence on bending angle and deposition area. Yarin [29] found that the bending instability is the result of competition of destabilizing electric force and stabilizing effect of the surface tension. Figure 7c shows the bending angle seemly kept constant, while the electric force varies with ambient RH levels. It suggests that RH has influence on surface tension.

PVP non-aqueous solutions

Experiments with PVP alcohol solutions were conducted to investigate separate influence of RH and evaporation rate on fiber diameters and process parameters, since evaporation rate of PVP alcohol solutions is independent on ambient RH level.

To understand the impact of RH on electrospinning process of PVP alcohol solutions, one series of experiments

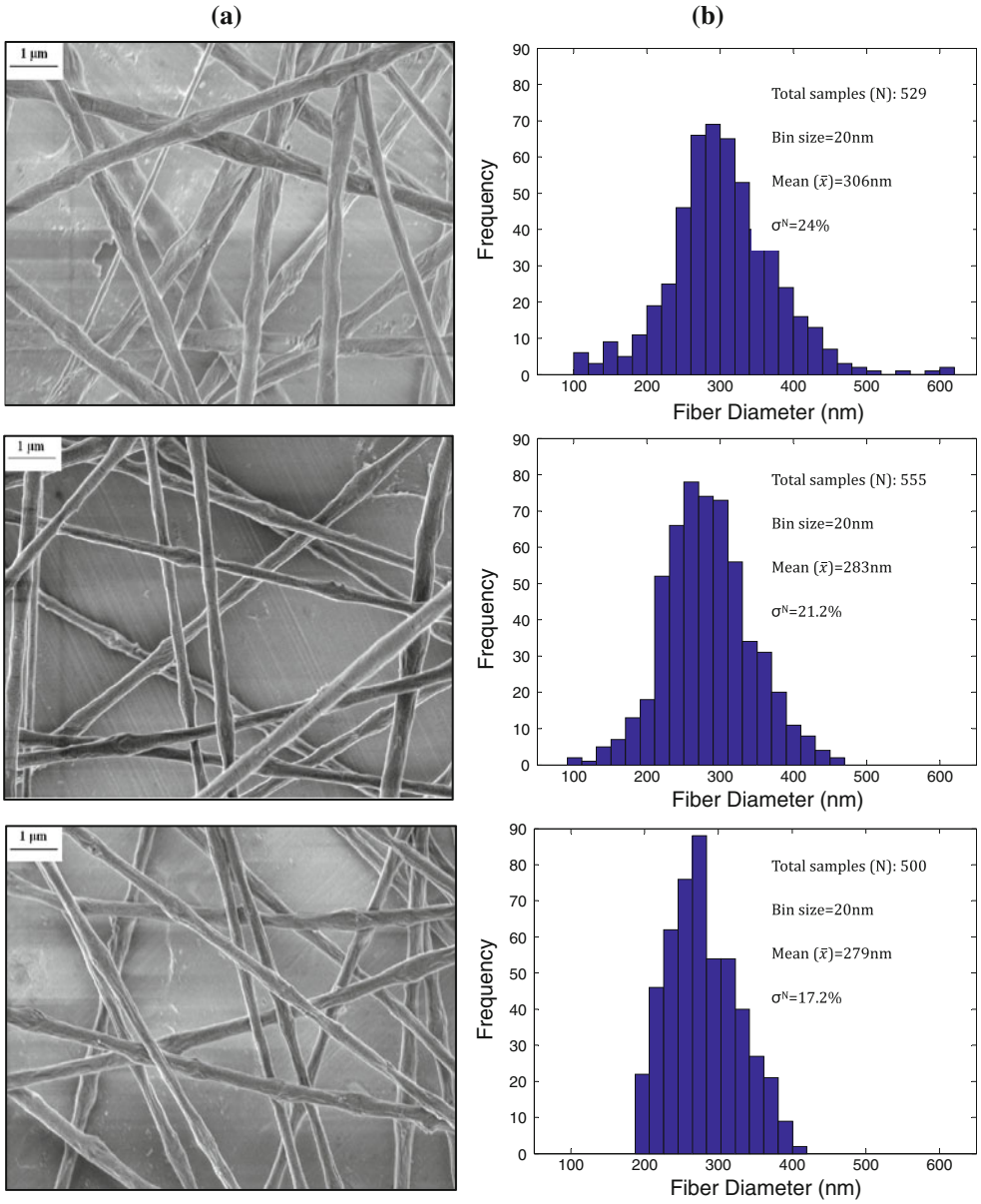

Fig. 5 **a** SEM images of electrospun nanofibers of 7 wt% PEO/water solutions for the voltage conditions in $V = 25.5$ kV (*up*); $V = 27.5$ kV (*middle*); $V = 30$ kV (*low*) ($Q = 0.042$ ml/min, *scale bar* = 1 μm). **b** Fiber diameter distributions of 7 wt% PEO/water solutions for the voltage conditions in (**a**): $V = 25.5$ kV (*up*); $V = 27.5$ kV (*middle*); $V = 30$ kV (*low*)

was conducted for 12 wt% PVP/ethanol for different ambient RH (Fig. 8). Fiber diameters of 12 wt% PVP/ethanol solutions decrease by ∼30 % as RH increases from 38 to 57 %. Similar to PEO/water solutions, both the current and fiber diameter of PVP/ethanol solutions decrease as RH increases.

The impact of RH on process parameters is shown in Fig. 9. Upper jet diameter increases 30 % and Taylor cone volume increases 180 %, which are consistent with the 33 % decrease of current as RH increases from 28 to 57 %. Compared to the results for PEO/water solutions, the increase of jet diameter is less than that of PEO/water solutions while the increase of Taylor cone volume is greater than that of PEO/water solutions. This suggests that the influence of RH on the electrospinning process of both PEO aqueous solutions and PVP alcohol solutions is significant.

For PVP/ethanol solutions, we observe that current decreases 33 % and fiber diameter decreases 66 % as RH increases 29 %, but this occurs for a constant evaporation rate. This effect was also observed by De Vrieze et al. [18]. One possible explanation he proposed is that RH still has an influence on the solidification rate of solutions. However, the evaporation rate of alcohol should be independent on ambient RH level. This indicates that besides the

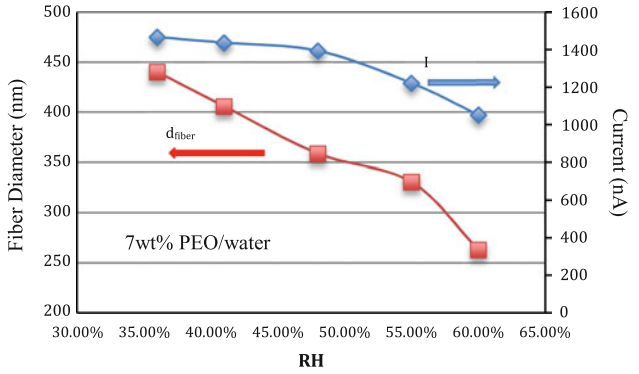

Fig. 6 Influence of RH on fiber diameters of 7 wt% PEO water solutions; fiber diameters decrease around 43 % as RH increases from 35 to 60 %. *Diamond* current (*I*), *square* fiber diameter (d_{fiber})

evaporation rate and solidification time, there is another significant factor that affects fiber diameter, which is influenced by ambient RH (possibly absorption of water).

In the next section, fiber diameters correlation is investigated in terms of measurable process parameters, evaporation rate, and ambient RH, from which not only fiber diameters can be predicted but also the physics of the influence of RH and evaporation rate on electrospinning process can be studied.

Prediction of fiber diameters based on process parameters, evaporation rate, and relative humidity

To understand the separate influences that RH and evaporation rate have on fiber diameter, correlations of charge density, jet diameter, evaporation rate, and ambient RH to fiber diameters for both PEO aqueous solutions and PVP alcohol solutions are studied. The investigation of the relation between process parameters and fiber diameters contributes to developing an understanding of the electrospinning process as well as determining what measurements could be measured in a real-time control system to insure desired fiber diameter.

Influence of RH for PEO aqueous solutions

Fridrikh et al. [21] analyzed the dynamic equations of Hohman et al. [15, 16] in terms of the whipping instability to develop a scaling law for fiber diameter. Evaluating the asymptotic balance between normal stresses due to surface tension and surface charge repulsion, he obtains:

$$d_{\text{fiber}} = \left(\gamma\bar{\varepsilon}\frac{Q^2}{I^2}\frac{2}{\pi(2\ln X - 3)}\right)^{1/3} \quad (2)$$

where γ is the surface tension (N/m); $\bar{\varepsilon}$ is the dielectric constant of ambient air; Q is the applied flow rate (m^3/s); I is the measured jet current (A); X is the dimensionless wavelength of the instability responsible for the normal displacements. Thus, it is expected that fiber diameter is proportional to $\left(\frac{I}{Q}\right)^{-2/3}$. This analysis has been experimentally confirmed by a log-log plot with PEO and PAN aqueous solutions [21, 30, 31]. The volumetric charge density (I/Q) has unit of (C/m^2), and reflects the strength of the electrostatic force acting on jet, which is the major thinning factor in electrospinning. However, the analysis does not include the influence of ambient RH.

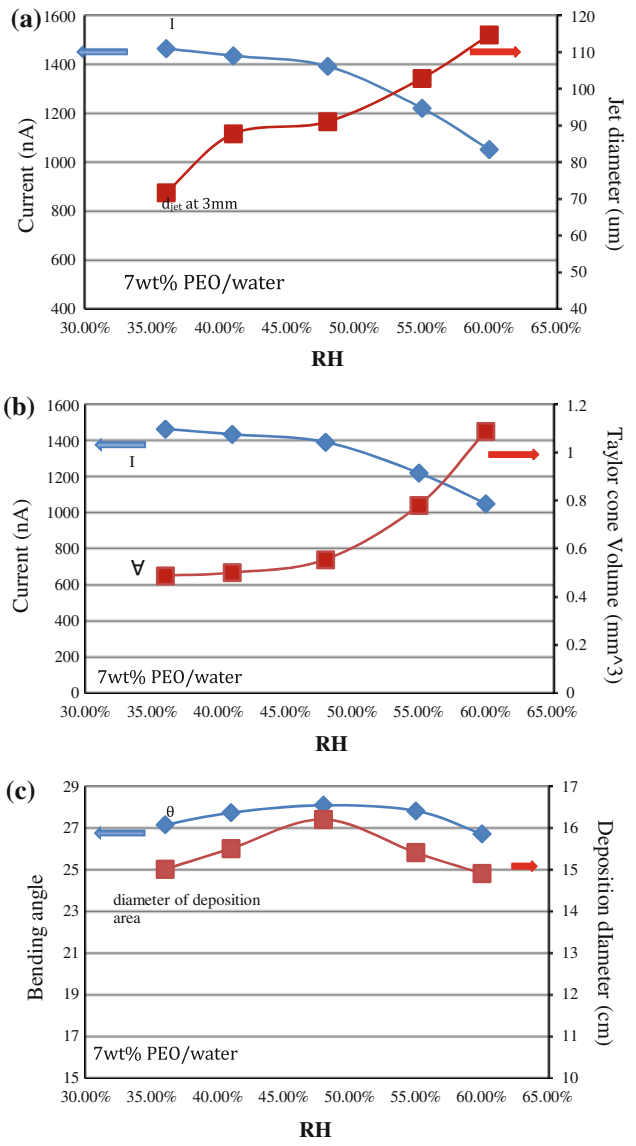

Fig. 7 **a** d_{jet} and current versus RH. *Diamond* current (*I*), *square* jet diameter (d_{jet}). **b** Taylor cone volume and current versus RH. *Diamond* current (*I*) *square* Taylor cone volume (∀). **c** Bending angle and deposition area versus RH. *Diamond* bending angle (θ), *square* deposition diameter

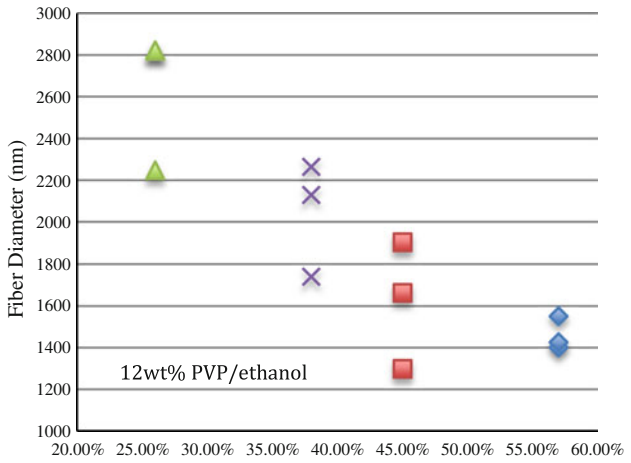

Fig. 8 Fiber diameters for 12 wt% PVP/ethanol solutions under different RH levels; fiber diameters decrease as RH increases. *Diamond* PVP/ethanol 57 %, *square* PVP/ethanol 45 %, *cross* PVP/ethanol 38 %, *triangle* PVP/ethanol 26 %

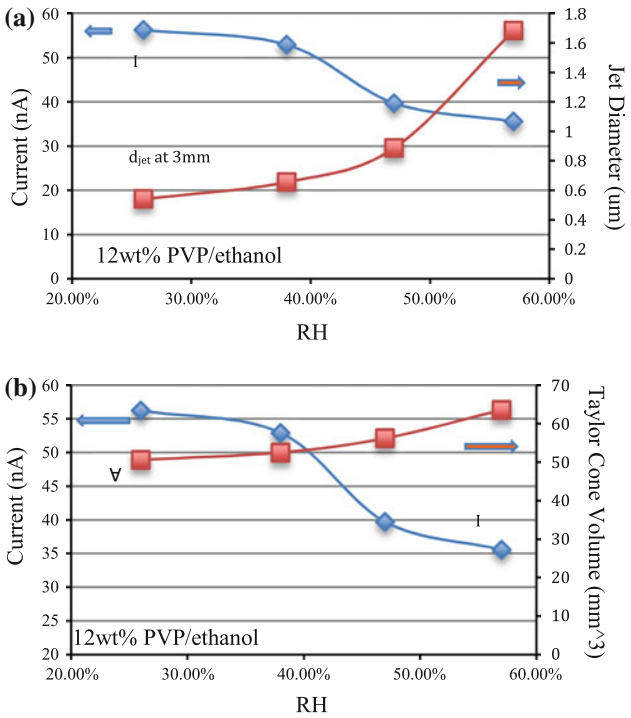

Fig. 9 Impact of RH on measurable parameters for 12 wt% PVP/ethanol solutions. **a** Jet diameter and current versus RH. *Diamond* current (I), *square* jet diameter (d_{jet}). **b** Taylor cone volume and current versus RH. *Diamond* current (I), *square* Taylor cone volume ($\forall$)

Figure 10 shows the correlation for our experimental data, conducted 7 wt% PEO water solutions for three different RH levels (30, 40, 55 %). Charge density does not provide a global correlation to fiber diameter for three different ambient RH levels. In addition, an overall slope for the data with different flow rates exists for each relative

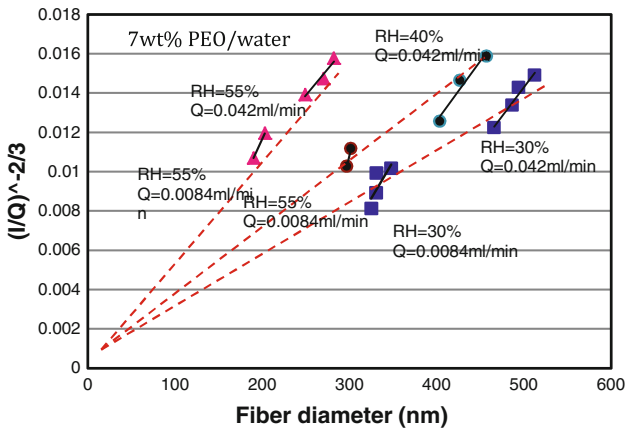

Fig. 10 correlation of charge density to fiber diameters for 7 wt% PEO water solutions at three different RH levels [26]. *Square* 30 %, *circle* 40 %, *triangle* 55 %

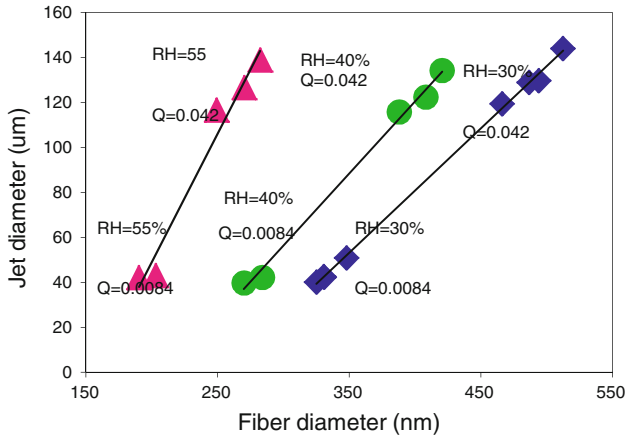

Fig. 11 Correlation of jet diameters and fiber diameters for 7 wt% PEO water solutions with three different ambient RH levels [26]. *Square* 30 %, *circle* 40 %, *triangle* 55 %

humidity, the local slopes of those data vary with flow rates [26]. In addition, Fig. 10 shows that flow rate also plays a role on fiber diameter. It is opposite to the fiber diameter correlation that Helgeson et al. [22] obtained, in which flow rate is not a determinant for fiber diameter.

Figure 11 shows the correlation of jet diameter (d_{jet}) to fiber diameter at different ambient RH levels. Similar to the charge density, there is a different correlation for different RH levels, but, for each RH level, it appears that the local slope is constant. This suggests that, by taking viscous force into account, for each ambient RH level, the local slopes of those data with different flow rates can be unified (although we need to obtain more data at intermediary points to fully confirm).

Taking the evaporation rate (1 − RH) into account and consider it as a fitting parameter, it is found that all data

collapse on a curve (Fig. 12). The curve indicates that there is a correlation between fiber diameter (d_{fiber}) and the measured jet diameter (d_{jet}) and RH, related to $d_{\text{jet}}(1-\text{RH})^4$. We note that other experimental factor does not yield a well-defined curve for the data.

In contrast, a similar correlation for charge density and RH to fiber diameter was attempted. The best curve fit is shown in Fig. 13. Here, a global correlation between fiber diameter (d_{fiber}) and the charge density and RH, given by $\left(\frac{I}{Q}\right)^{-2/3}(1-\text{RH})^{1.5}$ is observed. By taking ambient RH into account, all data points do collapse on a straight line, indicating that ambient RH contributes to a global correlation to fiber diameter. But, in contrast to the jet diameter correlation, the local slopes of different conditions vary, which is similar to what is achieved in only considering charge density (Fig. 10). Possibly, this occurs since charge density only reflects the dominant stretching force (electrical force), but has no relation with the retarding force (viscous force). It suggests that the good correlation of fiber diameter to jet diameter, shown in Fig. 12, occurs since the jet diameter represents the force balance in the jet and captures both the electrical force (stretching force) and the viscous force (retarding force).

To examine the impact of different terms, we consider Feng's [17] steady-state momentum analysis of the jet for Newtonian fluids in terms of a differential element given by:

$$\rho v\frac{\mathrm{d}v}{\mathrm{d}z} = \rho g + \frac{3\eta_0}{r^2}\frac{\mathrm{d}}{\mathrm{d}z}\left(r^2\frac{\mathrm{d}v}{\mathrm{d}z}\right) + \frac{\gamma}{r^2}\frac{\mathrm{d}r}{\mathrm{d}z} + \frac{\sigma}{\epsilon_0}\frac{\mathrm{d}\sigma}{\mathrm{d}z} + (\epsilon-\epsilon_0)E\frac{\mathrm{d}E}{\mathrm{d}z} + \frac{2\sigma E}{r} \quad (3)$$

(1) (a) (2) (3) (b) (4)

where (1) is the change of jet momentum; (2) viscous term; (3) surface tension term; (4) electrical term; (a) is the gravity term; (b) is the charge self-repulsion term; ρ is the density of solutions; v is the axial velocity of the short section of the jet; η_0 is the viscosity of solutions; r is the radius of the short section of the jet; γ is the surface tension; σ is the charge density of the short section of the jet; ε and ε_0 is the dielectric constants of the jet and the ambient air; E is the electrical field; z is the axial position of the short section of the jet.

To obtain a sense of dominant factors of Eq. (3), the terms (Table 2) are evaluated. For a 8 wt% PEO/water solution ($M_w = 400$ k) experiment, in the upper jet region (at 3 mm from the vertex of nozzle). Since the local electrical field (E) is considered as constant, which equals the external electrical field, the $\left((\epsilon-\epsilon_0)E\frac{\mathrm{d}E}{\mathrm{d}z}\right)$ is neglected. Table 2 indicates that in the upper jet region, the electrical force term and viscous force term are significant factors that affect jet stretching. The shear viscous force is determined by viscosity of solutions and velocity gradient ($\frac{\mathrm{d}v}{\mathrm{d}z}$). This indicates that for each RH level, the different viscous forces, which come from different flow rates, may result in different local slopes for different flow rates. However, the viscous force is only significant at the initial regime (between the nozzle regime and asymptotic regime, around 5 mm from vertex of needle), since the velocity gradient becomes smaller as the jet the stretches. After 5 cm from

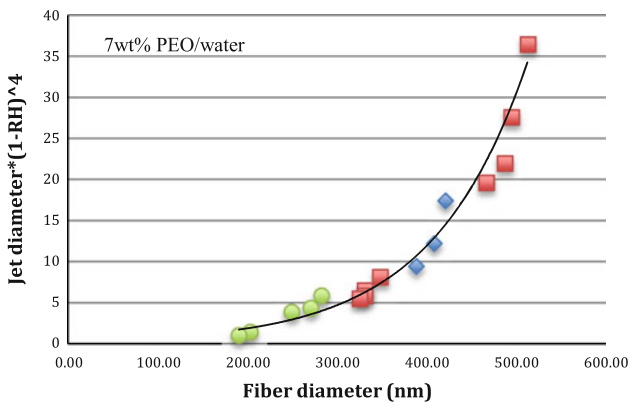

Fig. 12 Correlation of jet diameter, RH, and fiber diameters for 7 wt% PEO/water solutions with three different ambient RH levels. Data from Xuri's thesis [26]. *Square* 30 %, *circle* 40 %, *triangle* 55 %

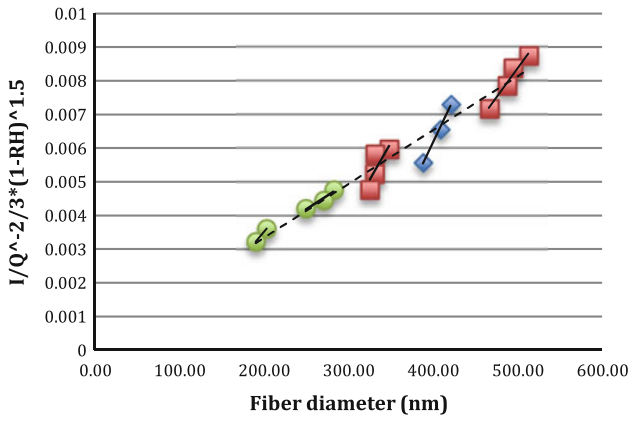

Fig. 13 Correlation of charge density and RH to fiber diameter for 7 wt% PEO/water solutions with three different ambient RH levels. Data from Xuri's thesis [26]. *Square* 30 %, *circle* 40 %, *triangle* 55 %

Table 2 Values of various force terms in the upper jet region at 3 mm from the vertex of nozzle

Force terms	Values (N/m^3)
Electrical term (4)	1.5×10^7
Viscous term (2)	1×10^7
Surface tension term (3)	1.5×10^5
Self-repulsion term (b)	3×10^6
Gravity term (a)	9800

8 wt% PEO/water solution, $M_w = 400$ k

the vertex of needle, the viscous force term ($\sim 4 \times 10^5$ N/m^3) is more than two magnitudes smaller than the electrical force term ($\sim 4 \times 10^7$ N/m^3) for 7 wt% PEO/water solutions. Hence, the viscous force only plays a role in the initial regime.

In the upper straight jet region (between the end of Taylor cone and the asymptotic regime), a balance between electrostatic and viscous terms (Rutledge, Fridrikh) suggests the following scaling law for jet diameter in this regime [23]:

$$d_{\text{jet}} = \left(\frac{6\upsilon Q^2}{\pi EI}\right)^{1/2} z^{-1} \quad (4)$$

where υ is the viscosity of solution (kg/(m s)); Q is the flow rate (m^3/s); E is the electrical field (V/m); I is the measured jet current (A); z is the upper jet diameter (d_{jet}) measured point (m). This relation indicates that jet diameter is determined by the force balance between the viscous force and the electrical force at the point measured in the upper jet. A possible explanation for the non-uniformity seen in Fig. 14 is that, in our research, jet diameter is measured at a fixed point related to the needle (3 mm below vertex of needle, at which jet diameter (~ 100 μm) can be measured accurately, since the resolution of our camera is 3.8 μm/pixel). We are currently evaluating how to specify an appropriate jet diameter measurement point.

For PEO/water solutions, the good correlation of fiber diameter to jet diameter (Fig. 12) indicates that RH plays a significant role on fiber diameters. However, the roles of ambient RH and evaporation rate in determining fiber diameter cannot be separated, since the evaporation rate of aqueous solutions is driven by ambient RH. Thus, in order to study their separate roles, we extend our experiments to PVP alcohol solutions.

Influence of RH and evaporation rate for PVP alcohol solutions

For non-aqueous solutions, the solvent evaporation rate is independent of ambient RH, so we can study the separate influence of RH and evaporation rate. Three different 12 wt% PVP/alcohol solutions were used with (ethanol, methanol and 1-butanol). These solutions have evaporation rate relative to water of 11, 7, and 1.5, respectively (in comparison, the evaporation rate of water at 60 % RH and 22 °C is 1). To examine the impact of evaporation rate on the electrospinning process, those three 12 wt% PVP/alcohol solutions were electrospun with different flow rates and voltages but constant ambient RH level (45 %). Figure 15 shows that charge density (I/Q) does not provide a good global correlation to fiber diameter, since, for each PVP alcohol solutions, the local slopes of those data for different flow rates are different. Figure 16 shows the correlation of jet diameter to fiber diameter, which reveals that the local slopes are uniform, but there is no overall correlation for all three solutions.

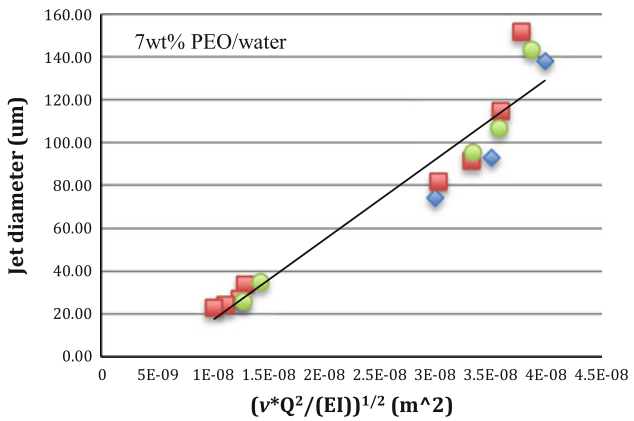

Fig. 14 Relation of jet diameter using Fridrich's nozzle/jet relations, in terms of charge density and viscosity for 7 % PEO/water solutions. Data from Xuri's thesis [26]. *Square* 30 %, *circle* 40 %, *triangle* 55 %

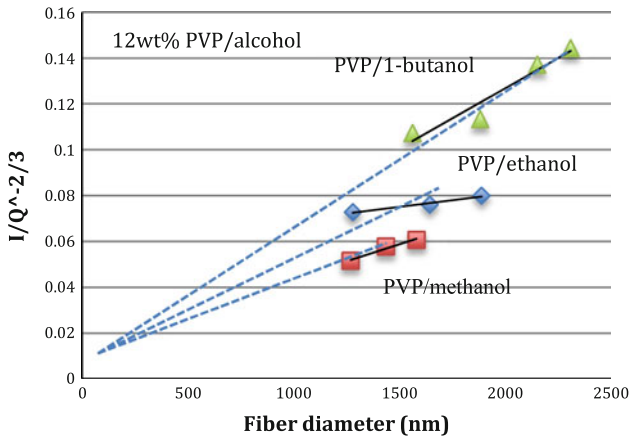

Fig. 15 Correlation of charge density to fiber diameter of three different 12 % PVP/alcohol solutions with constant ambient RH level (45 %). *Diamond* PVP/ethanol, *square* PVP/methanol, *triangle* PVP/1-butanol

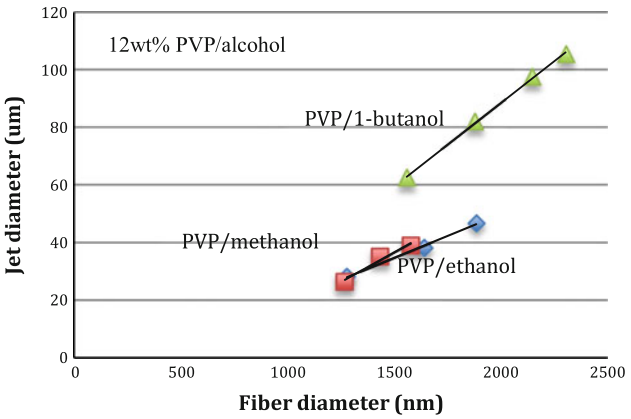

Fig. 16 Correlation of jet diameter to fiber diameter of three different 12 % PVP/alcohol solution with constant ambient RH level. *Diamond* PVP/ethanol, *square* PVP/methanol, *triangle* PVP/1-butanol

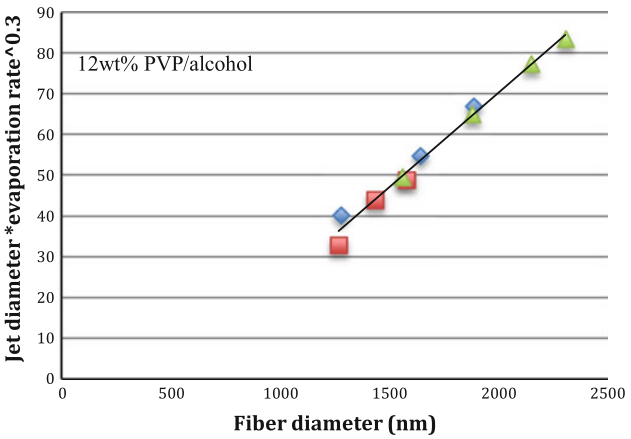

Fig. 17 Correlation of jet diameter and evaporation rate to fiber diameter of three different 12 % PVP/alcohol solutions with constant ambient RH level (45 %). *Diamond* PVP/ethanol, *square* PVP/methanol, *triangle* PVP/1-butanol

However, taking the different evaporation rate into account, a good fiber diameter correlation is found using jet diameter and solvent evaporation rate in terms of $d_{\text{jet}} \cdot \dot{m}_{\text{evap}}^{0.3}$, as shown in Fig. 17.

To investigate the impact of RH, the three different PVP/alcohol solutions were electrospun with different RH levels. Figure 18 shows correlations to fiber diameter using $(d_{\text{jet}} \cdot \dot{m}_{\text{evap}}^{0.3})$, which indicates that RH and evaporation rate have separate influence on fiber diameter. By taking RH into account, a good fiber correlation is obtained in terms of jet diameter, evaporation rate and RH, given by $d_{\text{jet}} \cdot \dot{m}_{\text{evap}}^{0.3} \cdot (1 - \text{RH})^2$ as shown in Fig. 19.

Comparing the power of the RH term $((1 - \text{RH})^2)$ with the power of the evaporation rate term $(\dot{m}_{\text{evap}}^{0.3})$ suggests that the influence of RH might be more than the impact that evaporation rate has on the electrospinning process.

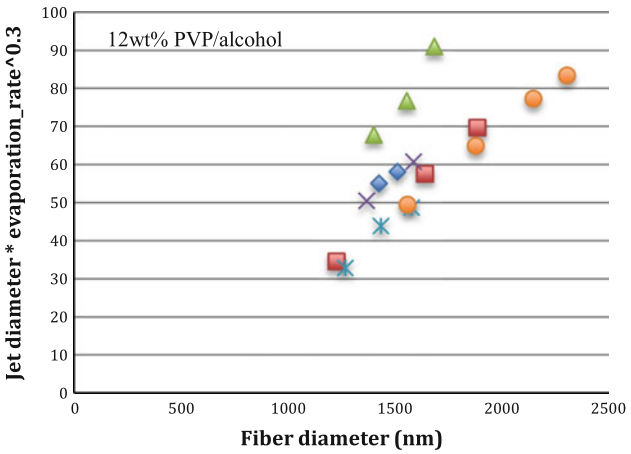

Fig. 18 Correlation of jet diameter and evaporation rate to fiber diameter of three different 12 % PVP/alcohol solutions with different ambient RH levels. *Diamond* PVP/ethanol 50 %, *square* PVP/ethanol 47 %, *triangle* PVP/ethanol 57 %, *cross* PVP/methanol 50 %, *asterisk* PVP/methanol 43 %, *circle* PVP/1-butanol 43 %

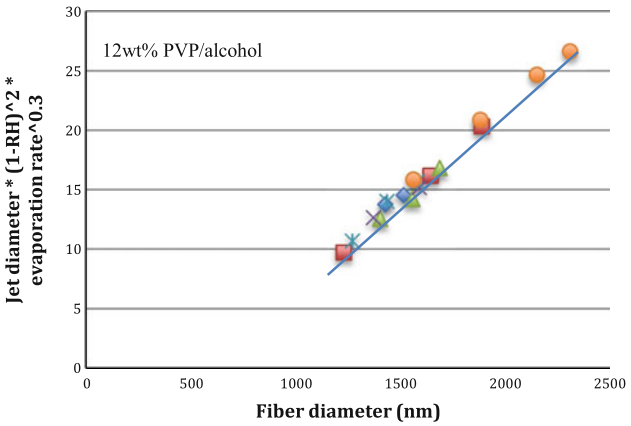

Fig. 19 Correlation of jet diameter, RH, and evaporation rate to fiber diameter of three different 12 % PVP/alcohol solutions with different ambient RH levels. *Diamond* PVP/ethanol RH 50 %, *square* PVP/ethanol RH 47 %, *triangle* PVP/ethanol RH 57 %, *cross* PVP/methanol RH 50 %, *asterisk* PVP/methanol RH 43 %, *circle* PVP/1-butanol RH 43 %

Evaporation rate represents a solution property; RH represents the ambient conditions; and jet diameter, reflecting force balance between electrical force (stretching force) and viscous force (retarding force), is determined by process conditions (applied voltage and flow rate) and solution properties (viscosity and conductivity). Thus it is not strange that fiber diameter of PVP alcohol solutions could be predicted by jet diameter, since the solution property, the process condition and the ambient environment condition are the main three parameter groups, which impact electrospinning process. Considering the conductivity and viscosity of those PVP alcohol solutions, it suggests that the fiber diameter correlation based on $(d_{\text{jet}} \cdot \dot{m}_{\text{evap}}^{0.3} \cdot (1 - \text{RH})^2)$ for PVP/alcohol solutions holds

for a large viscosity range from 0.38 to 3.02 Pa s and a large conductivity range from 0.1 to 3.3 μS/cm.

Figure 20 also suggests that, for PVP/alcohol solutions, jet diameter is also determined by electrical force and viscous force. An overall correlation of electrical force and viscous force to jet diameter exists. We investigate the reason of various local slopes, which might be the fixed jet diameter measurement point and the influence of RH on surface tension.

As discussed above, fiber diameter can be predicted by three measurable parameters, jet diameter, evaporation rate, and ambient RH. However, evaporation rate is determined by applied material. Then ambient RH and jet can be viewed as two controllable variations in the electrospinning process. Ambient RH can be controlled by several approaches, such as dry nitrogen flow, water vapor, and salt bath. On the other hand, the jet diameter is determined by experimental inputs (applied voltage and flow rate) and ambient RH level. Hence, operating regimes need to be developed to obtain required jet diameter.

Operating regime and closed-loop control system

Applied voltage is one of the major controllable inputs for the electrospinning process. In this study, a vision system, viewing the Taylor cone, is used to determine the upper and lower bounds of applied voltages for different flow rates with different ambient RH levels.

Investigation of operating regime

Figure 21 delineates the five distinct Taylor cone regimes identified for a flow rate, shown with the corresponding Taylor cone images as a function of the applied voltage. When the applied voltage is low, the electric force cannot overcome the surface tension of the fluid. No jet is ejected from the apex of the Taylor cone and the fluid builds up at the needle and falls in drops (regime 1 in Fig. 21). When the voltage is increased above a critical voltage, a liquid jet emerges. However, due to the low electric field strength and charge density, the rate at which the electric force removes fluid from the Taylor cone, cannot match the flow supply rate. Thus, fiber deposition is accompanied by droplets falling intermittently from the needle tip (regime 2 in Fig. 21). With increased voltage, a continuous jet occurs (regime 3 in Fig. 21). However, there is a large variation of Taylor cone volumes in this region. With a further increase of the voltage, the variation decreases significantly and its shape becomes more steady. Then, the electrospinning can be maintained stably for long periods with minimal process variations (regime 4 in Fig. 21). It is noted that the voltage range for this minimal jet fluctuation regime is a function of flow rate Q. It requires higher voltage for higher flow rate as shown by the dashed upper and lower lines in Fig. 21. If one does not determine these bounds and run the

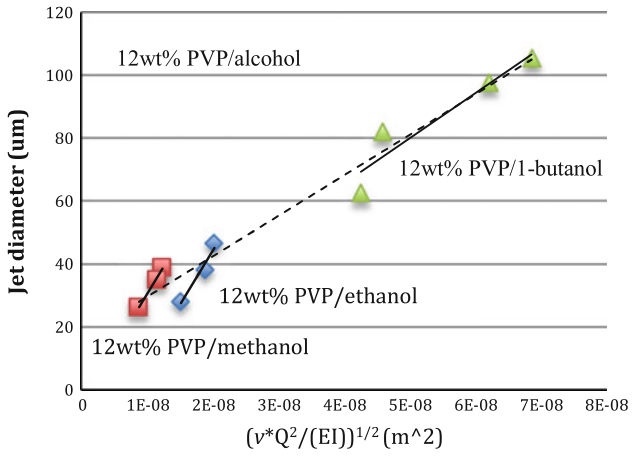

Fig. 20 Relation of jet diameter using Fridrich's nozzle/jet relations, in terms of charge density and viscosity for 12 wt% PVP/alcohol solutions. *Diamond* PVP/ethanol, *square* PVP/methanol RH 47 %, *triangle* PVP/1-butanol

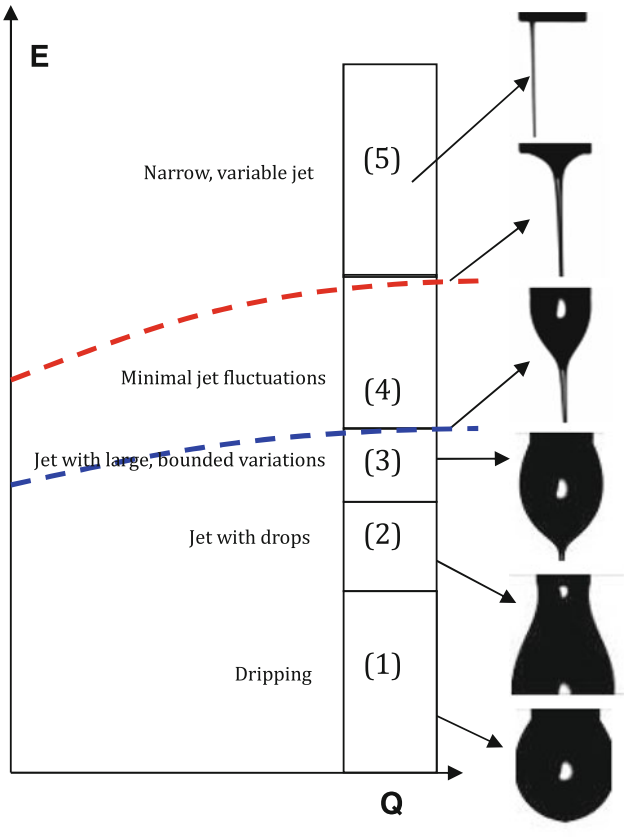

Fig. 21 Five electrospinning regimes identified by electric field strength and the corresponding Taylor *cone shapes*. *1* Dripping, *2* jet with drops, *3* jet with large, bounded variations, *4* minimal jet fluctuations, *5* narrow, variable jet

experiment within them, our results suggest that there will be a large variation in fiber diameter. For example, Huang et, al. had a large variation in fiber diameter distribution of PAN and PSU solutions [20]. The reason might be that they did not select an appropriate operating regime and were unable to maintain a constant Taylor cone volume.

In our study, we examine the operating regimes for different polymer solutions which have a significantly different parameter values in terms of conductivity, viscosity, and surface tension. For 5 % PEO ($M_w = 4 \times 10^5$) aqueous solutions, the lower and upper bounds of the operating regime in terms of voltages were determined for different flow rates (Fig. 22). The critical voltages for the bounds were normalized by the plate separation distance ($H = 35$ cm) and expressed as electric fields.

Figure 22 shows the operating regime in terms of electric field strength as a function of flow rate for 5 wt% PEO/water solution [26]. They are affected by the ambient conditions such as humidity, and even the setup geometry.

Operating regimes of 12 wt% PVP/alcohol solutions were also obtained with the same approach as PEO aqueous solutions. Operating regimes of 12 wt% PVP/ethanol, PVP/methanol, and PVP/1-butanol solutions are shown in Fig. 23. Because the conductivity, viscosity, and surface tension of 12 wt% PVP/alcohol solutions are different with those of 5 wt% PEO/water solutions, the lower bounds and upper bounds (determined in terms of minimal variation of Taylor cone volume) of 12 wt% PVP/alcohol solutions are lower than those of 5 wt% PEO/water solutions and the range of operating regime of 12 wt% PVP/alcohol solutions are also thinner than those of 5 wt% PEO/water solutions. And even for various PVP/alcohol solutions, the lower and upper bounds are also different, because of different material parameters.

Figures 7b and 9b show that Taylor cone volumes of both PEO/water solutions and PVP/alcohol solutions increase as ambient RH increases, since higher ambient RH leads to a decrease in current. Thus, the voltage settings for those operating regimes need to be increased with ambient RH increasing, in order to maintain the similar Taylor cone volume. Experiments were conducted by 6 wt% PEO/water solutions at two different ambient RH levels, 31 and 60 %. The images of the Taylor cone are shown in Fig. 24.

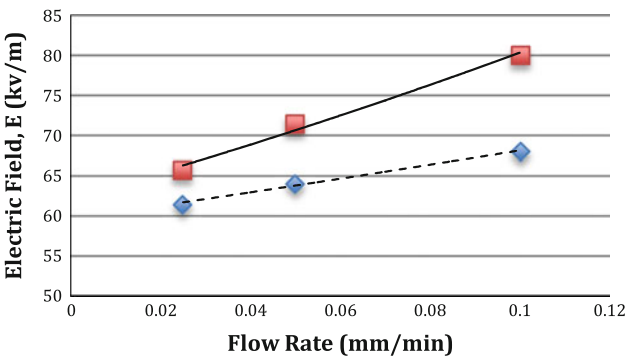

Fig. 22 Operating regime of 5 wt% PEO/water solution with constant ambient RH level (33 %)

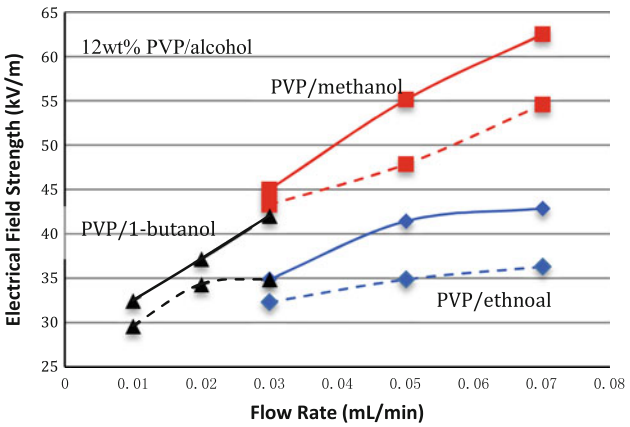

Fig. 23 Operating regime of 12 wt% PVP/alcohol solutions with constant ambient RH level (25 %). *Diamond* PVP/ethanol, *square* PVP/methanol RH 47 %, *triangle* PVP/1-butanol. *Dashed line* lower bound, *straight line* upper bound

Investigation of closed-loop control system

The study of fiber diameter correlations and operating regimes provide a basis for development of a closed-loop control system for electrospun nanofibers.

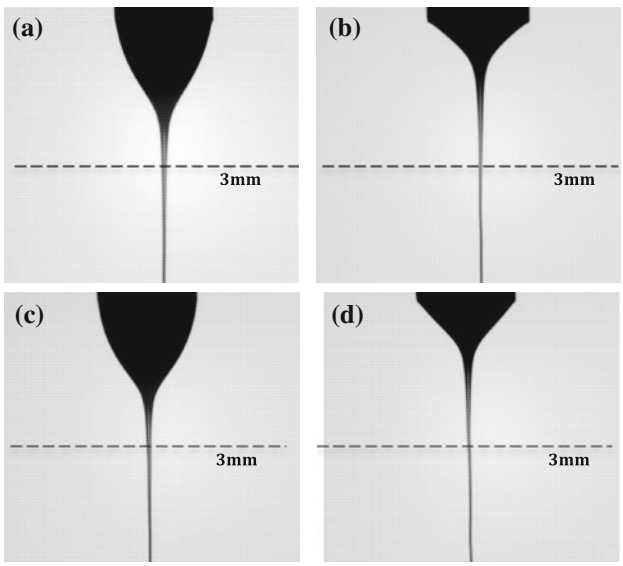

Fig. 24 The corresponding Taylor *cone shapes* of 6 wt% PEO/water solutions for the upper and lower bounds of operating regimes and the voltage conditions at $Q = 0.025$ ml/min. **a** RH = 31 %, $V = 22$ kV; **b** RH = 31 %, $V = 24$ kV; **c** RH = 60 %, $V = 24.2$ kV; **d** RH = 60 %, $V = 26$ kV. *Dashed line* measurement point of jet diameter (3 mm)

RH is a settable parameter

If ambient RH is a settable parameter, considering higher RH leads to thinner fiber diameter, an appropriate high RH level could be selected. Since high RH levels may lead to beads, too high RH levels cannot be selected. For 7 wt% PEO/water solutions, while RH is higher than 70 %, beads will appear on the fibers. After the ambient RH level is selected, the jet diameter can be determined by the response to the required fiber diameter according to fiber diameter correlation. Highest voltage should be selected based on the power of power supply. Then, according to the operating regime, a maximum flow rate could be selected to maximize the production rate tocalculate the jet diameter, which will result in desired fiber diameter.

RH is a disturbance

On the other hand, if ambient RH cannot be controlled. Then RH is considered as a disturbance of the electrospinning process and the required jet diameter, responding to the desired fiber diameter, should change with ambient RH. Then, the applied voltage and flow rate should also be adjusted to achieve the required jet diameter, in order to get desired fiber diameter and minimize the disturbance of ambient RH. However, because the operating regime is also dependent on ambient RH, it is hard to maintain the maximum production rate.

Based on the fiber diameter correlation and operating regime, a close-loop control system could be developed for electrospun nanofibers in the future.

Conclusion

This paper analyzes the impacts that evaporation rate and ambient relative humidity have on the electrospinning process for PEO/water and PVP/alcohol solutions. It is found that fiber diameter decreases as ambient RH increases, in spite of a corresponding decrease in current, which reduces stretching force. In terms of measurable process parameters, the upper jet diameter and the Taylor cone volume increase while ambient RH increases.

Two measurable process variables, charge density and upper jet diameter, were used to develop correlations to fiber diameter. An overall correlation is found in terms of charge density and ambient RH ($(1-\mathrm{RH})^{1.5}$) to fiber diameter, but there are local slope variations for different conditions. Using the upper jet diameter, a correlation is also obtained to fiber diameter for PEO aqueous solutions in terms of ambient RH ($(1-\mathrm{RH})^{4}$). The upper jet diameter could be considered as a measurable control variable because of its good correlation to fiber diameter as well as ease of measurement.

In order to separately understand the influences that evaporation rate and ambient RH have on fiber diameter, experiments of PVP alcohol solutions were also conducted. A good correlation of upper jet diameter, evaporation rate, and ambient RH to fiber diameter is found in terms of $(\dot{m}_{\mathrm{evap}}^{0.3})$ and $(1-\mathrm{RH})^{2}$. The power dependence indicates that for PVP alcohol solutions, the ambient RH has a greater impact on the process than evaporation rate.

The influence of applied voltage and RH to Taylor cone volume for different flow rates is also investigated to determine the operating regime. Combined with fiber diameter correlation, an appropriate operating regime can be selected. The selection of operating regime depends on if the ambient RH can be considered as a settable environmental parameter or as a disturbance acting on the process. The operating regime should be selected to achieve the desired fiber diameter while maximizing production rate.

Acknowledgements The authors are grateful to the funding support from the NSF (CMMI0826106) and Army (W911QY-11-1-0014), and the contributions of Thierry Desire, David Ouk, Sarah Provencher, Vicki Liu, and Michael Manion.

References

1. Doshi J, Reneker DH (1995) Electrost J 35:151
2. Srinivasan G, Reneker DH (1995) Polymer Int 36:195
3. Matthews JA et al (2002) Biomacromolecules 3:232
4. Matthews JA et al (2003) J Bioactive Compat Polym 18:125
5. Boland ED et al (2004) Front Biosci 9:1422
6. Kwoun SJ, Lec RM, Han B and Ko FK (2000) In: The 2000 IEEE/EIA International Frequency Control Symposium and Exhibition, 7–9 June, 2000. The Westin Crown Center, Kansas City, Missouri, USA
7. Wang XY et al (2002) Nano Lett 2:1273
8. Han L et al (2009) MRS Proceedings, Symposium WW: Polymer nanofibers—fundamental studies and emerging applications. doi:10.1557/PROC-1240-WW09-27
9. Mertz T et al (2011) MRS Proceedings, Symposium MM: Organic biolelectronics and photonics for sensing and regulation. doi:10.1557/opl.2011.877
10. Yan X, Gevelber M (2010) ASME dynamic systems and control conference, vol 2, p 51. doi:10.1115/DSCC2010-4201
11. Taylor GI (1966) Proc R Soc Lond Ser A 291:159
12. Yarin AL, Koombhongse S, Reneker DH (2007) Polymer 48:6913
13. Reneker DH, Yarin AL (2008) Polymer 49:2387
14. Yarin AL (1993) Free liquid jets and films: hydrodynamics and rheology. Longman/Wiley, Harlow/New York
15. Hohman MM et al (2001) Phys Fluids 13(8):2201
16. Hohman MM et al (2001) Phys Fluids 13(8):2221
17. Feng JJ (2002) Am Inst Phys. doi:10.1063/1.1510664
18. De Vrieze S et al (2009) J Mater Sci. doi:10.1007/s10853-008-3010-6

19. Tripatanasuwan S, Zhong Z, Reneker DH (2007) Polymer 48:5742. doi:10.1016/j.polymer.2007.07.045
20. Huang L et al (2011) J Polym Sci, Part B: Polym Phys 49:1734
21. Fridrikh SV et al (2003) Phys Rev Lett 90(14):144502
22. Helgeson ME et al (2006) Am Inst Chem Eng. doi:10.1002/aic.11056
23. Rutledge GC, Fridrikh SV (2007) Adv Drug Deliv Rev 59:1384
24. Yarin AL (2001) Am Inst Phys. doi:10.1063/1.1408260
25. Greenspan L (1997) J Res Natl Bur Stand A 81A:89
26. Yan X (2011) PhD thesis, Boston University
27. Yan X, Gevelber M (2010) J Electrost 68:458
28. Jayjock MA (1994) Am Ind Hyg Assoc J 55:230
29. Yarin AL (2001) Am Inst Phys. doi:10.1063/1.1333035
30. Shin YM et al (2001) Polymer 42(25):9955
31. Yu JH, Fridrikh SV, Rutledge GC (2006) Polymer 47(13):4789